# Nanodroplet-Based Super-Resolution Ultrasound Localization Microscopy

Ge Zhang [a, b, c 1], Chen Liao [a, d 1], Jun-Rui Hu [e, 1], Hai-Man Hu [f], Yu-Meng Lei [a, *], Sevan Harput [g, *], Hua-Rong Ye [a, *]

[a] Department of Medical Ultrasound, China Resources & Wisco General Hospital, Wuhan University of Science and Technology, Wuhan, China, 430080.

[b] Hubei Province Key Laboratory of Occupational Hazard Identification and Control, Wuhan University of science and technology, Wuhan, China, 430065.

[c] Physics for Medicine Paris, Inserm U1273, ESPCI Paris, PSL University, CNRS, Paris, France, 75015.

[d] Medical College, Wuhan University of Science and Technology, Wuhan, China, 430065.

[e] Department of Pharmacy, Union Hospital, Tongji Medical College, Huazhong University of Science and Technology, Wuhan, China, 430022.

[f] Department of Electrical and Electronic Engineering, Hubei University of Technology, Wuhan, China, 430068.

[g] Department of Electrical and Electronic Engineering, London South Bank University, London, UK, SE1 0AA.

[1] These authors contributed equally to this work

*** Corresponding author:**

yehuarong@hotmail.com（H.R. Ye）; harputs@lsbu.ac.uk (S. Harput);

leiyumeng0814@hotmail.com (Y.M. Lei)

## Highlights

- Ultrasound localization microscopy, as a microvascular imaging technique that enables early diagnosis and monitoring of various diseases.
- Nanodroplets have potential to speed up image acquisition time while ensuring image resolution.
- Ultrasound localization microscopy is required to offer a clear added value compared to the current clinical imaging techniques.

## Abstract

Over the last decade, super-resolution ultrasound localization microscopy (SR-ULM) has revolutionized the ultrasound imaging with its capability to resolve the microvascular structures below the ultrasound diffraction limit. The introduction of this imaging technique enables the visualization, quantification, and characterization of tissue microvasculature. The early implementations of SR-ULM utilize microbubbles (MBs) that require long image acquisition time due to the requirement of capturing sparsely isolated microbubble signals. The next generation SR-ULM employs nanodroplets that have the potential to significantly reduce the image acquisition time without sacrificing the resolution.

This article reviews various nanodroplet-based ultrasound localization microscopy techniques and their corresponding imaging mechanisms. A summary is given on the preclinical applications of SR-ULM with nanodroplets and the challenges in the clinical translation of nanodroplet-based SR-ULM are presented while discussing the future perspectives. In conclusion, ultrasound localization microscopy is a promising microvasculature imaging technology that can provide new diagnostic and prognostic information for a wide range of pathologies, such as cancer, heart conditions or

autoimmune diseases, and enable personalized treatment monitoring at micro-level.

**Keywords:** Nanodroplets, Microbubbles, Ultrasound Imaging, Ultrasound Localization Microscopy, Super-Resolution, Activation, Recondensation, Diagnosis, Therapy.

Optical localization microscopy (OLM), such as photo-activated localization microscopy (PALM) and stochastic reconstruction microscopy (STORM), has been demonstrated the capability to differentiate the plasma membranes and intracellular organelles at spatial resolutions below tens of nanometers [1]. The imaging mechanism of PALM is that the first laser pulse will activate a subgroup of fluorescent proteins within the molecules. Then the second laser pulse is used a new subgroup of fluorescent proteins [2]. After accumulating a stack of images, a spatiotemporal filter is applied to obtain the blinking fluorescent signals. Each spatially isolated fluorescent signal within every single image is localized as a localization event [3]. All localization events from all the images are then accumulated into the final super-resolution image. OLM has revolutionized optical fluorescent imaging by imaging intracellular organelles below the diffraction limit [4]. However, one of the major challenges of applying OLM is that organisms scatter the light significantly, which limits the penetration depth in biological tissues and makes in vivo imaging challenging [5].

Compared with optical pulses, acoustic wave is significantly less scattered in biological tissues in vivo and can be used to image deep structures. Microvascular changes in vivo are critical features in the visualization and characterization of various diseases, such as tumor angiogenesis, peripheral arterial disease, coronary heart disease, etc. Gas-filled microbubble contrast agents are utilized in clinically routine contrast-enhanced ultrasound (CEUS) examinations to enhance blood flow signals [6]. These microbubble contrast agents can generate strong resonant signals within the frequency range from 1 to 15 MHz compared with the tissue background, thereby to enhance the contrast of vasculature [7]. The blood pool contrast agents remain in the blood vessels and do not spread into the extravascular space. They are not absorbed by any tissue or cell and are rapidly cleared from the blood through the pulmonary [8; 9]. As a kind of pure blood pool contrast agent commonly used in clinics, it can provide basic information of relevant organs and vessels and visualize the degree of neovascularization of the lesions, which is helpful for the diagnosis and treatment of various diseases [10]. However, the corresponding axial resolution is limited by the half wavelength and there is a compromise between imaging resolution and penetration depth. The penetration depth is determined by the decay of the ultrasound, which decreases with frequency while the resolution increases with frequency, so the deeper penetration depth indicates a lower resolution [11]. Inspired by OLM, super-resolution ultrasound localization microscopy (SR-ULM) was performed using a relatively low concentration of flowing microbubble contrast agents to visualize microvasculature beyond image resolution limit [12]. The corresponding two-dimensional (2-D) and three-dimensional (3-D) SR-ULM techniques have shown promise in the previous studies using microbubble contrast agents.

Because microbubbles are sub-wavelength, ULM requires point spread function of single microbubble for precise localization. Localization error occurs because of highly overlapping regions of the concentrated microbubbles, and low concentration ensures that single microbubble signal can be distinguished and further the localization of microbubbles can be achieved [13]. Therefore, microbubble-based SR-ULM requires a relatively low concentrations of flowing microbubbles. Flow is crucial here because sparse activation of microbubbles is not possible unlike OLM. Such requirement for microbubble re-location or replenishment significantly increases ULM acquisition time, especially for microvasculature with relatively slow flow rates, such as capillary

networks, while nanodroplets are independent of flow rate [14, 15].

To overcome this challenge, previous studies have shown that a relatively high concentration of low-boiling-point nanodroplets can be randomly and sparsely activated within the clinical safety limits, and then deactivated as required by controlling the applied ultrasound amplitude, thus demonstrated the ultrasonic counterpart of PALM at depth [16; 17]. Nanodroplets are converted from liquid to microbubbles under acoustic or laser activation, and the resulting spatially stationary, temporally transient microbubbles will realize the formation of SR-ULM before re-condensation into liquid nanodroplets state [18]. Nanodroplets are disrupted by interleaved activation and imaging pulses. This enables the rapid sampling of different subpopulations of microbubbles between successive imaging frames. This may reduce the acquisition time and is unaffected by flow and concentration [16]. In addition to this, repeated activation and recondensation of high-boiling-point nanodroplets are possible, which demonstrates the feasibility of nanodroplet-based SR-ULM [19].

This article reviews various nanodroplet-based ultrasound localization microscopy techniques and their corresponding imaging mechanisms. In addition, we summarized the preclinical application and the challenges required to be overcome to promote clinical translation of nanodroplet-based ultrasound localization microscopy. Finally, the future perspective of this technique is discussed.

**Ultrasound Contrast Agents**

CEUS imaging is sensitive to tissue vasculature as the ultrasound contrast agents flow through. These contrast agents could highlight the microvasculature, as the ultrasound transducer is also sensitive to slowly moving microbubbles. With the rapid developments in the design of these ultrasound contrast agents, nanodroplet contrast agents can be manufactured via condensation and extrusion methods [20]. Compared to optical contrast agents, ultrasound contrast agents can travel deep within the tissues, which makes them advantageous in clinical contrast imaging modalities.

**Microbubbles.** Microbubble contrast agents have now developed to the third generation [21]. According to the different gas cores within the microbubbles, they are mainly air, nitrogen, carbon dioxide, fluorine sulfur gas, fluorine carbon gas, etc [22]. The first-generation ultrasound microbubble contrast agent has no shell and is mainly represented by air-filled microbubbles [23]. Their stabilities are relatively weak as they could not travel far within the vasculature after intravenous injection. Additionally, the in vivo circulation time is relatively short, which results in limited clinical applications. For example, the diffusion of contrast agent Levovist in blood is faster than the previous product. The former is air-based, where small molecules can easily diffuse into the blood stream through microbubbles [24]. A number of attempts has also been made by previous studies, such as manufacturing shells with polymer-based materials. However, these contrast agents were failed to be commercialized due to poor imaging quality [25]. Perfluorinated gas with low solubility in water replaced air as the second-generation microbubble contrast agent, and the shell material began to transform into liposomes， but it does not have specific targeting [26]. The third-generation ultrasound contrast microbubbles are drug-loaded microbubble with targeted function, which is used for diagnosis and treatment of diseases [27; 28]. Microbubbles with gaseous cores encapsulated by lipid shell layers are the most commonly used contrast agent in clinical CEUS examinations [29]. Microbubble contrast agents normally have a diameter ranged from 1 to 10 micrometers [30]. Therefore, they cannot travel outside the vasculature as the blood pool contrast agents.

At present, the commercialized microbubble contrast agents approved by FDA mainly include Sonovue (Bracco, Milano, Italy), Sonazoid (GE Healthcare, WI, USA) and Definity (Lanthus

Medical Imaging, MA, USA) [26]. Chen et al. performed preoperative lymphography enhanced ultrasound in patients with thyroid carcinoma using the microbubble contrast agent SonoVue to evaluate the ultrasound features of lymph nodes, the area of lymphatic drainage, and the detection of sentinel lymph node [8]. Olli et al. used the Sonazoid® contrast agent to perform CEUS of superficial lymphatic vessels in the upper extremities of the human [31]. It is potentially valuable in assessing the kinetics of lymph fluid and allowing imaging of abnormal lymphatic anatomy. Anton et al. applied carbon dioxide foam to ultrasound imaging of rat heart to achieve high ultrasound echoes. It minimizes tissue damage compared to iodine contrast agents [32]. At the same time, microbubbles are the most typical precursors of nanodroplets, which need to be further processed into nanodroplets through mechanical stirring, pressurization, condensation and other steps [33]. Researchers have shown that commercial and FDA-approved Definity (Lantheus Medical Imaging, Billerica, MA, USA) could be used to produce nanodroplets. The nanodroplets used by Lea-Bank are formed by Definity through agitation, pressurization, and other steps. It was proved to be a tool for neurosuppression and nerve stimulation [33]. Sheeran et al. directly applied the clinical contrast agent Definity to form nanodroplets through mechanical agitation [34]. With the rapid development of nanomedicine, nanobubbles can be a novel contrast agent. Nanobubbles, usually formed from lipid shells and perfluorocarbon gas cores, are 10 times smaller than the microbubbles. Nanobubbles are compared with microbubbles and usually have a low contrast signal, but are widely used in the treatment of various malignancies [35]. Nanobubbles have the potential to be extravasated into the tumor space due to their enhanced permeability and retention (EPR) effect. These extravasation potentials contribute to highly sensitive observations of tumor biomarkers, which are important for early cancer diagnosis [36; 37].

**Nanodroplets.** Recently, nanodroplet (ND) contrast agents have been widely investigated as these nanodroplets could offer more flexibility in ultrasound imaging compared to microbubbles. Nanodroplets normally have perfluorocarbon liquid core and are encapsulated by a lipid shell [38]. The advantages of using nanodroplet contrast agents in ultrasound imaging can be summarized below. First, it has been found in the previous study that, nanodroplet contrast agents have significantly longer half-lives in vivo compared to microbubble contrast agents. The microbubble half-life is usually 3-5min and the average half-life of nanodroplets is 30-60min [39]. Second, nanodroplet contrast agents can be spatiotemporally activated into microbubble contrast agents to selectively provide the ultrasound contrast signals, which offers more flexibility in real-time ultrasound imaging [40]. Due to the requirements for sparsity of flowing microbubbles, the microbubble-based ULM requires a long acquisition time, especially for small microvasculatures [41]. Since not all nanodroplets are activated at the same time, activating nanodroplets detected by ultrasound can be achieved at very high agent concentrations, both with or without flow [42]. When it comes to cancer imaging, nanodroplet-based ULM has the potential to offer enhanced insights into tumor angiogenesis, characterized by the presence of vessels with very slow flows [43]. Nanodroplets are invisible to ultrasound before activation, and when nanodroplets are acoustically or optically activated, they form transient microbubbles that immediately exhibit hyperechogenicity in ultrasound imaging, and as droplets are activated and deactivated at the ultrasound pulse repetition frequency, the signal can accumulate as quickly as sending imaging pulses, enabling fast cumulative localization, resulting in faster super-resolution imaging [44-46]. Third, the nanodroplets can extravasate into the cancerous space due to the leaky vasculature of cancerous endothelial wall and EPR effect, which make them useful in cancer extravasation imaging [35; 47; 48]. Many researches have

tried to verify that nanodroplets can extravasate within a range of sizes, usually with the optimum exosmosis size of 100 to 300 nm [49; 50]. Rapoport et al. performed experiments on mouse thigh subcutaneous muscle and adipose tissue under a microscope and observed the vasculature and found that the extravasation rate of nanodroplets into the normal tissue was very slow [51]. Song R. et al. have demonstrated that cavitation-facilitated permeability enhanced across the blood-brain barrier in rats induced by acoustically vaporized nanodroplets [52]. This indicates that phase change nanodroplets can be used as a safe, efficient, and durable reagent to achieve satisfactory cavitation mediated permeability enhancement in biomedical applications. Due to the limited capacity to load therapeutic agents, short in vivo circulation time, it is difficult for microbubble contrast agents to achieve effective drug concentration in the tumor site. However, previous studies have demonstrated that drug-loaded nanodroplets could be aggregated in the tumor site by enhancing permeability and retention effects. Additionally, it could open the blood-brain barrier to achieve drug delivery in the brain. These nanodroplets can be converted into microbubbles under targeted ultrasound irradiation and release therapeutic drugs within the microbubbles [33; 38]. It alleviated some of the cytotoxic effects of conventional chemotherapeutic agents on healthy cells. Therefore, drug-loaded nanodroplets could provide better tumor treatment and imaging methods due to the advantages of strong drug-carrying capacity, long half-life, and the ability to reach out the extravascular space [53]. Ho et al. applied doxorubicin-loaded nanodroplets and ultrasound to treat tumor-bearing mice, which improved the therapeutic efficacy [54]. Lea-Banks et al. injected decafluorobutane nanodroplets loaded with drug-mimicking dye into rats and exposed their brain to ultrasound. The dye was found to penetrate through the blood-brain barrier and be retained locally in the brain tissue. Therefore, this proved the capability of drug-loaded nanodroplets to open the blood-brain barrier and deliver drugs [55].

Finally, compared to microbubbles, nanodroplets can selectively enhance and observe the blood supply of a single vessel of interest and its downstream vessels [40]. Because nanodroplets need to be activated and deactivated by ultrasound, and nanodroplets with different boiling points require different acoustic energies. In many previous studies, nanodroplets were classified according to their boiling points. Tianqi Xu et al. investigated and compared the cavitation characteristics of flowing low and high boiling-point phase-shift nanodroplets during focused ultrasound exposures [56]. Meanwhile, Christian T McHugh et al. pointed out that the cavitation of nanodroplets with high boiling point requires high acoustic pressures while the nanodroplets with low boiling point will be converted into microbubbles at lower acoustic pressures [57]. So this review will classify nanodroplets according to boiling point. We present the activation conditions and situations of various types of nanodroplets in Table 1.

Table 1. The activation conditions and situations of various nanodroplets in key studies

| Core | Concentration (droplets/mL) | Temperature (°C) | Size (nm) | Mechanical index | Number of cycle | Ref. |
|---|---|---|---|---|---|---|
| Octafluo-ropropane | $1.0 \times 10^9$ | 37 | 350 | 0.2 | 1 | 58 |
| Decafluo-robutane | $1.8 \times 10^8$ | 37 | 119 | 1.3 | 1-2 | 16 |

| | | | | | | |
|---|---|---|---|---|---|---|
| Perfluoro-hexane, Perfluoro-butane | $2.0 \times 10^9$ | 37 | 202-420 | 1.1-1.7 | 2-4 | [19] |
| Octafluo-ropropane | $3.3 \times 10^9$ | 24 | 153 | 0.8 | 1 | [45] |

**Low-Boiling-Point Nanodroplets.** Low-boiling-point nanodroplets normally include octafluoropropane ($C_3F_8$, OFP) -based and decafluorobutane ($C_4F_{10}$, DFB) -based nanodroplets as described in the previous studies [59]. As can be seen from Table 2, OFP and DFB have relatively lower boiling point compared to perfluorohexane ($C_6F_{14}$, PFH) [60]. Therefore, they have relatively lower activation threshold thus they can be activated into microbubble contrast agents via diagnostic ultrasound pulses at depth [45]. It was found in the previous literature that, the activation threshold for activating OFP nanodroplet is 0.14 mechanical index (MI) whereas that for activating DFB nanodroplet is 0.40 MI [20].

Table 2. The characteristic parameters of various nanodroplet used in different nanodroplet-based ultrasound localization microscopy.

| **Chemical formula** | **Name** | **Molecular weight (g/mol)** | **Boiling point (℃)** | **Spatial resolution (μm)** | **Temporal resolution (Hz)** | **Activation conditions** | **Application** | **Ref.** |
|---|---|---|---|---|---|---|---|---|
| $C_6F_{14}$ | Perfluoro-hexane (PFH) | 338 | 56 | 7-16 | Several hundred | Laser | Imaging of the mouse brain | [61] |
| $C_6F_{14}$, $C_4F_{10}$ | Perfluoro-hexane (PFH), Decafluo-robutane (DFB) | 338, 238 | 56, -2 | 64 | 100 | Acoustic | Imaging of the rabbit quadriceps muscle | [19] |
| $C_4F_{10}$ | Decafluo-robutane (DFB) | 238 | -2 | 40 | 1000 | Acoustic | Visualization of rabbit renal microvas-culature | [17] |
| $C_3F_8$, $C_4F_{10}$ | Octafluo-ropropane (OFP), Decafluo-robutane (DFB) | 188, 238 | −37, -2 | 115 | 500 – 10000 | Acoustic | Imaging of the rabbit renal microvas-culature | [42] |

The low-boiling-point nanodroplet can be manufactured by condensing and pressurizing microbubble contrast agents. Briefly, the vial containing the microbubbles was kept submerged in an ice-salt bath and then pressurized with ambient air into the vial as shown in the Figure 1 below. The advantage of using low-boiling-point nanodroplets compared to high-boiling-point nanodroplets is that, the low-boiling-point nanodroplet can be relatively easily activated to microbubble contrast agents via acoustic pulses within a clinical safety level [16; 45; 62-64]. However, as a lower boiling-point liquid core is used, spontaneous vaporization may happen as they are not very stable under the physiological temperature. It was found in the previous study that the spontaneous vaporization of low-boiling-point nanodroplets may help with ULM processing as it could potentially provide additional localizations [45].

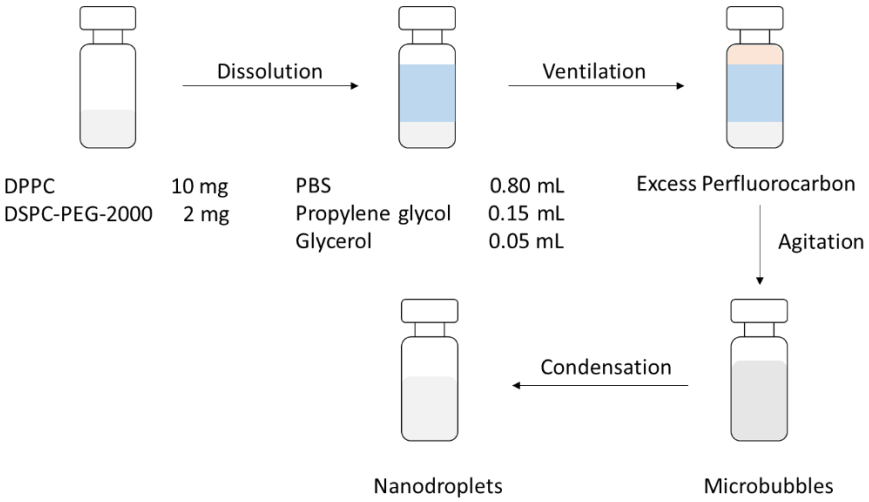


Figure 1. The manufacturing process of low-boiling-point nanodroplets.

**High-Boiling-Point Nanodroplets.** Previous study has demonstrated that the application of high-boiling-point nanodroplets (Perfluorohexane, $C_6F_{14}$) in SR-ULM [61]. Compared to the low-boiling-point nanodroplets (Decafluorobutane, $C_4F_{10}$), perfluorohexane-based nanodroplets have a significantly higher activation threshold, therefore, they require much higher energy to be activated to microbubbles. In a number of previous studies, both acoustic and photo-energies were used to assisted in the activation of the high-boiling-point nanodroplets [61; 65-67]. Luke et al. used laser energy to activate high boiling point perfluorocarbon nanodroplets to image the brains of a mice that have undergone craniotomy [61]. Yoon et al. used laser energy to activate perfluorohexane nanodroplets for super-resolution imaging [67]. Zhang et al. used acoustic energy to activate octafluoropropane nanodroplets for ultrasound super-resolution images[68]. However, the advantage of using high-boiling-point nanodroplets compared to the low-boiling-point nanodroplets is that they behave significantly stable under the physiological temperature [69].

**Principles of Ultrasound Localization Microscopy**

**Principle and Trilemma of Microbubble-based ULM.** For microbubble-based SR-ULM, low concentrations of microbubbles are required for localization processing. Then the dynamic video of microbubble flow is obtained either in B-mode or contrast mode. Then a crucial part of ultrasound localization processing is to distinguish microbubbles from the surrounding tissue. Clutter filtering technique was used enhance the contrast signals and suppress the background tissue signals. Once obtained these filtered contrast signals, these spatially isolated signals were localized. As the point

spread function of the imaging system can define the acoustic response to a single isolated point scatterer, the coordinates of each signal can be identified, and its accuracy is significantly higher than the diffraction-limited resolution [14]. After the localization processing, these localized signals between the consecutive frames can be tracked to define the paths and velocity of microbubbles within the microvasculature.

In practice, microbubble-based SR-ULM imaging requires to compromise imaging speed, fidelity and resolution as shown in Figure 2. With the improvement of image acquisition speed, the image resolution of microvasculature will be sacrificed. The improvement of microvascular image resolution will affect the degree of image expression of microvasculature.

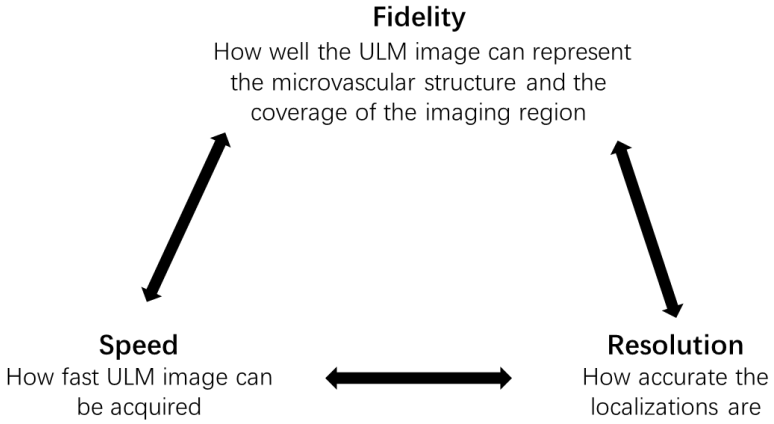


Figure 2. Compromise between fidelity, speed and resolution in the generation of SR-ULM.

Injection of low-concentration microbubbles can achieve better resolution but a longer imaging time [70]. The image acquisition can be done faster by injecting a higher concentration of MBs, which sacrifices the resolution [71]. Another option is just acquiring for a shorter period of time using a low MBs concentration while achieving a good resolution, however this reduces the fidelity of the final SR images and the diagnostic quality [72; 73]. In conclusion, MB-based SR imaging has the trilemma given above [41; 74]. Any method, algorithm or technique that breaks or bends this triangle is a big step forward in SR-ULM[75; 76].

Nanodroplets are the arguably the best solution to this trilemma, as they can be injected in high concentration and activated stochastically on demand, therefore which accelerates the image acquisition speed while covering the whole imaging area[42]. Since the activations of nanodroplets are performed in a stochastic fashion and only a small subset of nanodroplets are activated at a given time, a high imaging resolution can be achieved through accurate localizations.

**Principle and Application of Low-Boiling-Point Nanodroplet-based ULM.** There are several schemes for low-boiling-point nanodroplet-based ULM such as acoustic wave sparsely activated localization microscopy (AWSALM), fast-AWSALM, the localization of the acoustic droplet vaporization signal, etc. We present two of them here, AWSALM (Figure 3) and fast-AWSALM (Figure 4). The basic imaging mechanism of AWSALM is that a subgroup of nanodroplets was sparsely activated by the first focus-wave activation pulse, because only the most easily activated nanodroplets were activated by selective activation pulse pressure[12]. Until the next upcoming activation pulse, these activated nanodroplets will produce acoustic signals. First, the existing activated nanodroplets generated by the previous activation pulse will be destroyed [68]; Second, a new subgroup of nanodroplets will be activated[42]. The localizations of different subgroups of

activated nanodroplets can be offered by this continuous activation and subsequent imaging pulses. Zhang et al prepared decafluorobutane nanodroplets and verified that AWSALM utilizes acoustic waves to sparsely and stochastically activate nanodroplets by acoustic vaporization and to simultaneously deactivate the existing vaporized nanodroplets via acoustic destruction. in a crossed-tube phantom [16]. Their team also extended the application of AWSALM to the animal, the in vivo ULM of a rabbit kidney microvessels was obtained within 1.1 seconds [17]. Zhang et al. developed fast-AWSALM with low boiling point octafluoropropane nanodroplets and high frame rate plane waves for simultaneous activation, destruction, and imaging to achieve ULM on a sub-second timescale [45; 66]. As the AWSALM technology, the technology does not require flow.

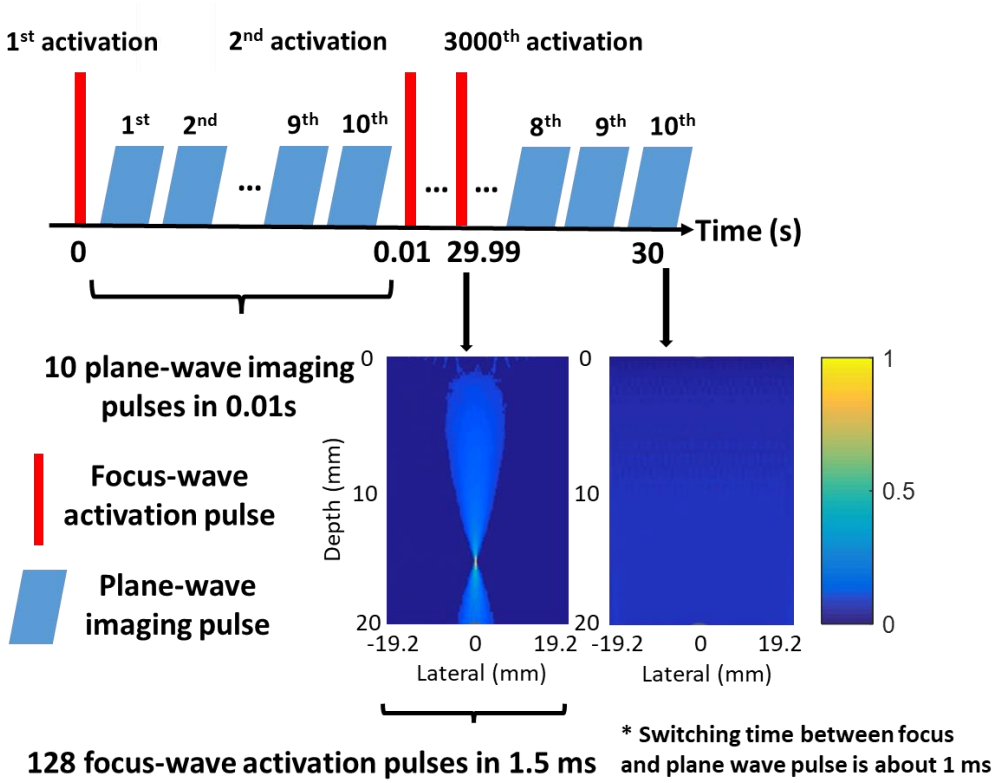


Figure 3. The illustration of "AWSALM" ultrasound pulse sequence.

The imaging mechanism of fast-AWSALM is different from that of AWSALM as fast-AWSALM utilizes plane-wave pulses for both activation and imaging of nanodroplets [66]. Due to the lower activation threshold of low boiling point nanodroplets, the acoustic pressure provided by the plane wave imaging pulse is sufficient to activate it for imaging [45; 64]. With plane waves, faster imaging and activation acquisition can be achieved without using focus-wave. Since merely the most easily activated droplets are activated by selected acoustic pressure, the subgroup of octafluoropropane nanodroplets will be sparsely activated by the first plane-wave imaging pulse, which is the principle of fast AWSALM[42]. These activated droplets will generate contrast signals until the next plane-wave pulse. There are three purposes of using these image pulses. The first purpose is to generate images, the second purpose is that a large number of the existing microbubbles activated by the previous pulse will be destroyed, and the third purpose is that a new subgroup of droplets will be activated into microbubbles. This continuous imaging, activation, and destruction pulses enable to offer different localizations of various subgroups of activated droplets within the region of interest.

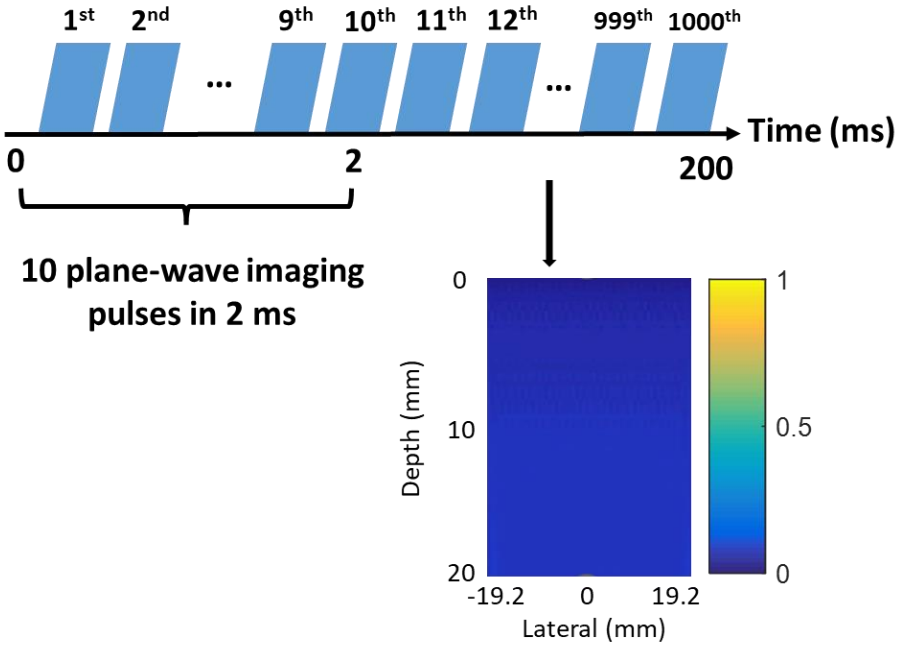


Figure 4. The illustration of "Fast-AWSALM" ultrasound pulse sequence.

**Principle and Application of High-Boiling-Point Nanodroplet-based ULM.** Previous study has demonstrated that the use of high-boiling-point nanodroplets for ULM. And nanodroplets are sparsely and randomly activated by optical or acoustic to reconstruct fine structures of the tissues. These high-boiling-point nanodroplets are made of a perfluorohexane liquid core encapsulated by a lipid shell and photoabsorbers to enable optical triggerin [77]. Due to the incorporation of the fluorosurfactant shell and near-infrared dye, these nanodroplets can be optically activated repeatedly [65]. Nanodroplets with perfluorocarbon-filled core and a shell of lipid and Pluronic F68, can undergo reversible vaporization and reliquefaction when driven by clinically safe acoustic pulses (MI :1.1−1.7). Therefore, a reversible phase transition can occur between the liquid and gaseous states to achieve multiple activations. Dong et al has shown that using these high-boiling-point nanodroplets can reconstruct ULM image of the non-flow tube phantom [19]. Therefore, the spatially isolated and temporally transient microbubbles offer high acoustic signals before recondensing to their original liquid state. The recondensation of high-boiling-point nanodroplets is a stochastic process. This means that at any given time, only a sparse subset of nanodorplets goes through the gas-to-liquid transition. This process may be propelled by a combination of the particle size, laser energy, amount of encapsulated dye, local pressure, and ambient temperature. Therefore, as long as the imaging frame rate is sufficiently high, the response of individual nanodroplet can be isolated by obtaining the difference between adjacent frames [67]. All the responses can be localized and then summed up to generate the final ULM image [16].

Dong et al. performed three criteria for the implementation of SR-ULM using the kind of blinking acoustic agent. First, the processes of activation and recondensation of these nanodroplets require to be reversible and the process of activation requires to be purely controlled by acoustic pulses from the same ultrasound imaging transducer used for imaging acquisition. Second, the acoustic pressure for the nanodroplet activation requires to be below the diagnostic limit. Third, the sparse and stochastic activation and recondensation signals requires to achieve high reconstruction

efficiency for SR-ULM [19]. These nanodroplets overcome the main limitations of localization imaging based on microbubbles, so that vascular imaging, especially small vessels, is no longer confused by slow blood flow. In addition, it only needs 100 frames of ultrasound imaging, which is an order of magnitude less than the conventional SR-ULM, and is enough to reconstruct the ULM without flow through cumulative localization or temporal radial autocorrelation. Compared to the low-boiling-point nanodroplets, the purpose is to detect the spatially isolated recondensation events for localizations. Additionally, this technique does not rely on flow. However, the activation of a number of high-boiling-point nanodroplets (eg. Perfluorohexane nanodroplets) requires the assistance of laser pulses, as their activation thresholds are relatively high compared to the other nanodroplets with lower-boiling-points [61]. This limits the penetration depth since laser pulse can only penetrate a few millimeters in tissue.

**Preclinical and Clinical Applications of ULM**

**Early Detection of Cancer.** Early detection of cancer found by medical imaging methods, while tumors are still small and before metastasis, will greatly increase the chances of successful treatment [78; 79]. Key information about the efficacy of the therapeutic approach is offered by imaging during treatment. Due to the low cost, wide accessibility and safety, ultrasound has the latent capacity to turn into the preferred method of cancer imaging [80]. Doppler ultrasound techniques or conventional B-mode are challenged to demonstrate microvascular characteristics on the scale of early tumor angiogenesis. ULM is not limited to diffraction-limited resolution, which makes this technique a potentially forceful implement [81; 82]. Lin and his research team successfully imaged the tumor microvasculature of rat subcutaneous fibrosarcoma tumors using ULM and evaluated the tumor-related angiogenesis. Compared with conventional ultrasound, the resolution was improved by 10 time [83]. This technology can be used to detect tumor-related angiogenesis, even though in deep tissues, malignancies can be distinguished by their angiogenic fingerprint [84]. In subsequent studies, Lin et al. observed 3-D microvascular patterns of rat subcutaneous fibrosarcoma tumor with ULM, and at the same time compared the microvascular characteristics with the control healthy tissues [78]. The curvature of blood vessels in tumor-bearing mice is significantly higher than that in the control group, and the degree of vascular heterogeneity is higher. This technology has the potential to distinguish between healthy and diseased tissues, and detect tumor-related angiogenesis. The changes of lymph node microcirculation often indicate metastasis. The identification and quantification of metastatic lymph nodes are crucial for tumor prognosis and treatment. Zhu et al. performed ULM on rabbit popliteal lymph nodes and realized the quantification of microvascular structure and blood flow dynamics of lymph nodes [85]. ULM can not only provide tumor microvascular information, but also measure the hypoxia state of tumor. Matthew et al. successfully imaged xenogeneic renal cell carcinoma growing on the chorioallantoic membrane of chicken embryo using ULM, evaluated the microvascular structure, vascular perfusion and hypoxia state of the tumor. They found that the microvascular signal in the center of the tumor was generally lower than that around the tumor, and showed a corresponding high degree of hypoxia probe expression, which was not obvious in conventional ultrasound contrast processing. It was found that the vessel curvature was significantly correlated with the quantity of hypoxia probe [86]. Zhang et al. successfully imaged human thyroid nodules and breast masses with ULM, and obtained useful clinical information such as microvascular flow rate and microvessel density, which is helpful for the differential diagnosis of benign and malignant [87; 88]. Different types of tumors can be distinguished by the fine details of vascular network provided by ULM. Opacic et al. used motion

model ULM to image breast cancer mice with different vascular phenotypes, extracted new super-resolution imaging parameters, including relative blood volume (rBV), blood flow direction and velocity, distance between blood vessel. They evaluated and verified these parameters with high-resolution **micro-computed tomography (micro-CT)** scanning and histological analysis of tumor slices, proved that the technology can identify tumors with different vascular phenotypes [89]. In addition, ULM has great potential in monitoring the response of early tumors to drug therapy. Ghosh et al. imaged breast cancer-bearing mice before and after administration, and found that there were an acute microvascular response within 2 hours after administration, which was verified with the results of immunohistochemistry. They also evaluated the longitudinal changes of tumor microvascular network in the response to vascular targeted drug therapy [90].

**Tissue Characterization.** Nanodroplet-based ULM is currently used for study in vitro and in animal since there is no commercial nanodroplet contrast agents approved by FDA [91]. With the development of nanodroplet-based ULM, this imaging technique can be used to display the microvasculature of various organs in vivo with faster imaging acquisition [92]. Kai et al. demonstrated that ULM showed diastolic and systolic perfusion in the microvasculature of rabbit kidney by using sono-switchable nanodroplets, and found that the spatial resolution was improved by four times [42]. Geoffrey et al. used high-boiling-point perfluorocarbon nanodroplet-based as "blinking" contrast agent to image the brain microvasculature of a craniotomy mouse and found that an axial resolution of 8μm and a lateral resolution of 16μm can be achieved in vivo, which is significantly better than that of conventional ultrasound imaging [61]. Dong et al. used laser-activated high-boiling-point nanodroplet-based ULM to show the microvasculature of quadriceps femoris in the hind leg of Japanese white rabbits [19]. The result demonstrated that laser-activated nanodroplet-based ULM in image reconstruction reduced the number of frames an order of magnitude than that in conventional ULM. Zhang et al. displayed the microvascular structure of rabbit kidney with the AWSALM technology based on the activation and deactivation of nanodroplets [17]. The result showed that the in vivo super-localization image can be obtained in 1.1 seconds using AWSALM.

**Diagnosis of Vascular Diseases.** Changes in microvascular structure, flow rate and other indicators often indicate the emergence of diseases, such as major diseases related to diabetes, atherosclerosis and so on. Changes in microvascular indicators often precede changes in the large blood vessels. Early monitoring and evaluation of the microvascular system facilitates early diagnosis and treatment of disease [43]. ULM has broken through the acoustic diffraction limit, significantly improved the spatial resolution, and is able to evaluate the early changes of microvasculature, thus improves the ability of disease monitoring and diagnosis [93]. Chen et al. successfully identified the rabbit femoral artery and its surrounding neovascularization using ULM. They observed the density of neovascularization and its related characteristics in the attachment of atherosclerotic plaque in rabbits, and performed micro-CT imaging, histopathological and morphological verification [94]. Qian et al. used the ULM technology to image the deep tissue of rabbit's eyes with high resolution, evaluated the microvasculature and flow velocity, and detected the subtle changes of blood flow. Which has great potential in detecting and monitoring eye diseases such as glaucoma in the future [95]. Ghosh et al. successfully used ULM to image the skeletal muscle microvasculature of type 2 diabetes mice, and compared them with lean mice to evaluate the structure and parameters of microvasculature, which is a new method for measuring the characteristics of skeletal muscle microvasculature and the dysfunction of type 2 diabetes [96]. In addition, ULM is also used to evaluate the changes of renal microvasculature. Chen et al.

successfully imaged the renal microvasculature of mice 21 and 42 days post-ischemia-reperfusion injury using ULM, and non-invasive quantified the changes of renal microvasculature in mice, which has great potential for future evaluation of progressive renal diseases [97]. Matthew et al. successfully imaged the brain microvasculature of aging mice by using the technology of ULM, provided the microvascular structure and function information of the cerebral microvasculature. They also quantified the differences in cerebral vascularity, blood velocity, and vessel tortuosity across several brain regions. Compared with young mice, the blood flow velocity and the blood volume of the cerebral cortex of aging mice was significantly reduced, while the blood vessel curvature was significantly increased [98]. These findings show that ULM technology has great potential in disease diagnosis and monitoring as shown in Table 3. In addition to the above-mentioned research in microvascular diseases in animals, ULM technique was also applied to image carotid artery, lower limbs, liver, kidney, pancreas and the other organs in human to prove the feasibility of performing ULM in deep tissues in human [99-102]. Due to the limitations such as long acquisition time and out-of-plane movement, further technical improvements are required to achieve better clinical results and wider range of applications.

Table 3. Summary of key researches on ultrasound localization microscopy in disease diagnosis and monitoring.

| Number | Object | Model | Application | Ref. |
|---|---|---|---|---|
| 1 | Subcutaneous fibrosarcoma | Rat | Evaluation of tumor-related microvasculature | 78 |
| 2 | Popliteal lymph nodes | Rabbit | Quantification of microvasculature and blood flow dynamics | 83 |
| 3 | A renal cell carcinoma xenograft model | Chicken embryos | Evaluation of hypoxia status of tumor | 86 |
| 4 | Thyroid nodules | Human | Differentiation of benign and malignant | 87 |
| 5 | Breast cancer | Mice | Differentiation of tumors with different vascular phenotypes | 89 |
| 6 | Breast cancer | Mice | Monitor the early response to drug treatment | 90 |
| 7 | Atherosclerotic plaque | Rabbit | Provision of neovascular density and related characteristics | 94 |
| 8 | Deep ocular tissue | Rabbit | Evaluation of microvessel and blood flow velocity | 95 |
| 9 | Skeletal muscle | Type 2 diabetes mice | Evaluation of microvasculature structure and parameters | 96 |

**Detection and Diagnosis of Arthritis.** Microvascular endothelial dysfunction is an early and/or important event in the development of cardiovascular disease and related organ damage, and also exists in patients with rheumatoid arthritis (RA) [103]. Fluorescent dye labeled hyaluronic acid is fixed

on the surface of nanoparticles and can be used as nanoprobe and contrast agent to selectively detect target molecules and diagnose the progress of RA [104-106]. In addition, due to the infiltration of abnormal blood vessels and inflammatory cells, the vascular permeability of RA site was significantly improved. Through the EPR effect, nanoparticles infiltrated into synovial tissue through the gap between endothelial cells and slowly released drugs [107]. The combination of passive targeting and EPR effect can maximize the effect of drug treatment [108]. The specific ligand recognized by cells at RA site is combined with the receptor on the surface of nanoparticles to selectively deliver the drug to the expected action site while further reduce the drug retention in normal tissues [109]. Compared with traditional therapeutic drugs, it has less toxicity and adverse side effects [110]. Although ULM has not been applied to the detection of microvasculature related to RA, it is believed that nanodroplet-based ULM has the potential to provide key information in the diagnosis and treatment of RA.

**Discussion**

ULM can provide comprehensive and quantitative microvascular parameters non-invasively and has great value in monitoring the diagnosis and treatment of microvascular diseases, such as the diagnosis and efficacy evaluation of tumors, chronic kidney diseases, inflammation, arteriolosclerosis, diabetes, etc [111]. ULM using contrast agents has display its tremendous latent capacity.

Previous studies have discussed different types of ULM based on nanodroplets, which can be activated by laser or ultrasound, respectively. For example, Luke et al. developed a transient laser-activated nanodroplet-based ULM and used it to image the brain of mice. The nanodroplets could be located within several micrometers, which is beneficial to achieve high resolution molecular imaging at substantial depth in tissue [61]. Dong et al. introduced a type of blinking acoustic nanodroplets, which could achieve ULM imaging at quite high concentrations and have much higher efficiency of repetitive activation [19]. Tang and his team developed nanodroplet-based AWSALM and fast-AWSALM, and further verified the ability to visualize microvasculature in vivo and in vitro, respectively, which opens the possibilities for super-resolution molecular imaging [16; 17; 42]. Nevertheless, there are a few challenges to be conquered to speed up the clinical translation of ULM. Out-of-plane motion, long acquisition time, and low frame rates are the major challenges faced by the clinical translation of ULM [43; 112-114]. A previous study has attempted to overcome out-of-plane motion by implementing 3D imaging technique [78]**.** The microbubble-based ULM results in long image acquisition time due to differentiation of individual microbubble signals. However, the nanodroplets-based ULM can significantly shorten image acquisition time by sparsely activating nanodroplets and deactivating nanodroplets as required [16]. Despite the fact that the super-resolution imaging quality may be poor due to the low imaging frame rate on clinical imaging systems, there are increasingly more new generation ultrasound systems that could support high-frame-rate imaging [100].

However, with all of these challenges, ULM has also been implemented on patients. Although these challenges may lead to imaging which are less accurate, the results in the previous studies have shown the significance of this technique [87; 88]. Due to the lack of a gold standard, verifying the accuracy of super-resolution ultrasound imaging (SRUS) in reliable clinical applications remains a well-recognized challenge. At present, several studies have applied a number of techniques (confocal microscopy, two-photon microscopy, micro-CT, etc) to evaluate the accuracy of ULM in the detection of microvascular. In vivo, the quality of the super-resolved images is often evaluated

through the self-coherence of the vessel branching pattern [43]. Christensen-Jeffries et al. compared optical images with super-resolution images of the same plane where shallow microvascular networks were observed. To determine the accuracy of ULM in the shallow tissues, it can be compared to established microscopy techniques such as confocal microscopy or two-photon microscopy [115]. Opacic et al. compared the level of tumor vascularization obtained by mULM to rBV values obtained by maximum intensity over time (MIOT) postprocessing, ex vivo micro-CT, and immunohistochemical (IHC) analysis of the tumor sections. The average speed obtained by motion model ULM was compared by them with the average speed calculated by the complementary dynamics. The quantitative values of the distance (mean, variance and maximum) to the nearest vessel obtained by IHC and mULM were compared by them [89]. Several studies have used micro-CT and histopathological examination to verify the authenticity of ULM microvascular detection [97; 116].

A recent study in the field of SR-ULM is about the development of machine learning algorithms. Due to the overlap of high concentration microbubbles, noise, tissue artifacts and motion in the image, SR-ULM image quality and spatial resolution can be reduced and localization error can be increased [13; 117]. Applying machine learning can identify and reject non-single microbubble echoes and filter artifacts and noise in the images. In nanodroplet-based SR-ULM techniques, nanodroplets will activate into microbubbles at lower MI and bring them to a moderate concentration. Therefore, applying machine learning will bring the same filtering, detection and localization effects to the activated nanodroplets [118].

One of the challenges for nanodroplet-based ultrasound localization microscopy is that all the nanodroplet contrast agents used in the previous literatures were manufactured in the lab. It means none of them has gone through the clinical trials. This is due to the fact that the nanodroplet contrast agents have not been FDA approved because it may induce biological effects. Previous study has demonstrated that the activation process of smaller nanodroplets may cause damage to the surrounding tissues, because the acoustic pressure and temperature required to activate the droplets increase as the particle size decreases [38]. The clincial translation of nanodroplets-based ULM still requires efforts. To this day, the application of ultrasound localization microscopy has been confirmed in a number of preclinical studies and different animal models. Nanodroplet contrast agents with different liquid cores have been developed, so that the corresponding activation mechanism can be comprehended. Nevertheless, a better normalization of activation strategies is expected to accelerate the clinical translation of nanodroplet-based SR-ULM. This is because the development of clinical grade ultrasound contrast agents demands large-scale and extensive clinical trials to prove the safety issues. Testing the biological effects of nanodroplet activation by hematology and histology found that no biological effects caused by nanodroplet activation were observed in the case of low MI [119]. For the nanodroplet contrast agents, they still require large-scale clinical trials. This is to prove its applicability in human body, so as to make further efforts for the acceleration of clinical translation. In addition, the academic research of newly discovered nanodroplet contrast agents faces a challenge, which is to generally supply industrial support for Phase II/III clinical trials. This makes it harder to narrow down the gap in clinical translation.

Another challenge is that the current activation strategies reported in the literature may be difficult to be integrated into the clinical ultrasound system. A number of studies utilized the laser energy to aid activating nanodroplets. However, it is challenging to integrate laser emission into the clinical ultrasound examination routine and this may also make the imaging procedures more complicated

for ultrasound sonographers. Most of the studies utilized the “Imaging + Activation” ultrasound pulse sequences to obtain the activated droplet signals. However, the current clinical ultrasound systems do not have the corresponding pulse sequences to support the activation of nanodroplets, which requires further improvements. The last concern about the nanodroplet-based ULM is the safety issue regarding the acoustic energy required to activate the nanodroplets. The FDA approved mechanical index (MI) value of 1.9 is the maximum threshold for diagnostic imaging. Currently, the MI used in all ultrasound super-resolution studies is within the range defined by the FDA, and the acoustic pressure range is 0-5MPa [16; 19; 45; 68]. Although this technique has been widely investigated in preclinical studies, a number of challenges still exist. For instance, out-of-plane motion, long acquisition time, low frame rates and no clinically available nanodroplets, these are the difficulties in the clinical translation of nanodroplet-based ULM at present. However, with the continuous investigations and efforts, it is believed that this technique may potentially be utilized in clinical diagnosis.

**Conclusion**

Driven by the novel design of advanced imaging sequences, development of high frame-rate ultrasound systems and ultrasound contrast agents, ultrasound localization microscopy has demonstrated its tremendous latent capacity in many clinical and preclinical studies by expanding the application of conventional ultrasound imaging techniques. It has been shown that the application of these various ultrasound contrast agents in early cancer diagnosis and sonodynamic therapy is feasible. With the rapid development of molecular chemistry, imaging processing techniques and ultrasonic physics, ultrasound localization microscopy is expected to become a highly sensitive and specific imaging tool. This will help clinicians better diagnose and manage diseases. Nevertheless, in order to be widely accepted by clinicians, these ultrasound localization microscopy techniques need to provide a distinguishable added value compared with current clinical ultrasound imaging techniques. Therefore, academic researchers and pharmaceutical companies need to jointly promote the translational process to accelerate the clinical translation.

In summary, nanodroplet-based SR-ULM was developed to produce ultrasound super-resolution images in sub-second scale. This is several orders of magnitude faster than the existing microbubble-based SR-ULM. Compared with microbubble contrast agent, the size of nanodroplets is significantly smaller. This indicates that this technique can potentially resolve the structure, which is beyond the scope of the current microbubble-based SR-ULM approaches.

**Declaration of competing interest**

The authors declare that they have no known competing financial interests or personal relationships that could have appeared to influence the work reported in this paper.

**Acknowledgement**

The authors would like to thank the helps from Prof. Mengxing Tang and Prof. Christopher Dunsby at Imperial College London in the completion of this article and the reviewers for reviewing this article. This work was supported by Hubei Province Key Laboratory of Occupational Hazard Identification and Control, Wuhan University of Science and Technology (No: OHIC2022Y02 and No: OHIC2022G06).

**Vocabulary**

Ultrasound imaging, a medical imaging technique using high-frequency sound waves to produce echoes in the body; ultrasound contrast agent, a solution that can enhance blood flow signals after intravenous administration; ultrasound localization microscopy,

an imaging technique for breaking the ultrasound diffraction limit to display the microvasculature within tissues by locating and tracking the ultrasound contrast agent; microbubble contrast agent, an ultrasound contrast agent filled with a gas core; nanodroplet contrast agent, a phase change ultrasound contrast agent, usually with a perfluorocarbon liquid core and encapsulated in a lipid shell; activation, the process of converting nanodroplets from liquid droplets to gaseous bubbles under acoustic or optical emissions.

**Reference**


1 JOHNNY, TAM, DAVID & MERINO Stochastic optical reconstruction microscopy (STORM) in comparison with stimulated emission depletion (STED) and other imaging methods. Journal of *Neurochemistry*, **2015,** *135*, 643-658.

2 BETZIG, E., PATTERSON, G. H., SOUGRAT, R., LINDWASSER, O. W., OLENYCH, S., BONIFACINO, J. S., DAVIDSON, M. W., LIPPINCOTT-SCHWARTZ, J. & HESS, H. F. Imaging intracellular fluorescent proteins at nanometer resolution. *science*, **2006**, *313,* 1642-1645.

3 BACH, J. N., GIACOMELLI, G. & BRAMKAMP, M. Sample Preparation and Choice of Fluorophores for Single and Dual Color Photo-Activated Localization Microscopy (PALM) with Bacterial Cells. *Methods Mol Biol*. **2017,** *1563*, 129-141.

4 LU, M., KAMINSKI, C. F. & SCHIERLE, G. S. K. Advanced fluorescence imaging of in situ protein aggregation. *Phys Biol*. **2020**, *17*, 021001.

5 AHN, C., HWANG, B., NAM, K., JIN, H., WOO, T. & PARK, J.-H. Overcoming the penetration depth limit in optical microscopy: Adaptive optics and wavefront shaping. *Journal of Innovative Optical Health Sciences,* **2019**, *12*.

6 GREIS, C. Quantitative evaluation of microvascular blood flow by contrast-enhanced ultrasound (CEUS). *Clinical Hemorheology & Microcirculation*, **2011** ,*49*, 137.

7 MEHTA, K. S., LEE, J. J., TAHA, A. A., AVGERINOS, E. & CHAER, R. A. Vascular applications of contrast-enhanced ultrasound imaging. *Journal of Vascular Surgery*, **2017**.

8 CHEN, L., DONG, B., JIANG, L., ZHANG, J., CHEN, L., LI, T., SHAO, Y. & SUN, X. Microbubble contrast agent SonoVue: An efficient medium for the preoperative lymphatic mapping of thyroid carcinoma. *Frontiers in Bioengineering and Biotechnology,* **2022**, *10.*

9 BARR, R. G., HUANG, P., LUO, Y., XIE, X., ZHENG, R., YAN, K., JING, X., LUO, Y., XU, H. & FEI, X. Contrast-enhanced ultrasound imaging of the liver: a review of the clinical evidence for SonoVue and Sonazoid. *Abdominal Radiology*, **2020**, *45*, 3779-3788.

10 AJMAL, S. Contrast-enhanced ultrasonography: review and applications. *Cureus*. **2021**, *13*.

11 MAMOU, J., KETTERLING, J. A. & SILVERMAN, R. H. Chirp-coded excitation imaging with a high-frequency ultrasound annular array. *IEEE transactions on ultrasonics, ferroelectrics, and frequency control*. **2008**, *55*, 508-513.

12 ZHANG, G., HARPUT, S., SHAH, A., HERNáNDEZ-GIL, J., ZHU, J., CHRISTENSEN-JEFFRIES, K., BROWN, J., LONG, N. J., ECKERSLEY, R. J. & DUNSBY, C. Photoacoustic Super-Resolution Imaging using Laser Activation of Low-Boiling-Point Dye-Coated Nanodroplets in vitro and in vivo. *IEEE International Ultrasonics Symposium (IUS)*, **2019**

13VAN SLOUN, R. J., SOLOMON, O., BRUCE, M., KHAING, Z. Z., ELDAR, Y. C. & MISCHI, M. Deep learning for super-resolution vascular ultrasound imaging. *IEEE International Conference on Acoustics, Speech and Signal Processing (ICASSP)*, **2019,** 1055-1059.

14 BURGESS, M. T., ALIABOUZAR, M., AGUILAR, C., FABIILLI, M. L. & KETTERLING, J. A. Slow-Flow Ultrasound Localization Microscopy Using Recondensation of Perfluoropentane Nanodroplets. *Ultrasound in Medicine & Biology*, **2022**, *48*, 743-759.
15 HUANG, C., LOWERISON, M. R., TRZASKO, J. D., MANDUCA, A., BRESLER, Y., TANG, S., GONG, P., LOK, U.-W., SONG, P. & CHEN, S. Short acquisition time super-resolution ultrasound microvessel imaging via microbubble separation. *Scientific reports*, **2020**, *10*, 1-13.
16 ZHANG, G., HARPUT, S., LIN, S., CHRISTENSEN-JEFFRIES, K., LEOW, C. H., BROWN, J., DUNSBY, C., ECKERSLEY, R. J. & TANG, M.-X. Acoustic wave sparsely activated localization microscopy (AWSALM): Super-resolution ultrasound imaging using acoustic activation and deactivation of nanodroplets. *Applied Physics Letters*, **2018**, *113,* 014101.
17 ZHANG, G., HARPUT, S., TOULEMONDE, M., BROUGHTON-VENNER, J., ZHU, J., RIEMER, K., CHRISTENSEN-JEFFRIES, K., BROWN, J., ECKERSLEY, R. J. & WEINBERG, P. Acoustic Wave Sparsely-Activated Localization Microscopy (AWSALM): In Vivo Fast Ultrasound Super-Resolution Imaging using Nanodroplets. *IEEE International Ultrasonics Symposium (IUS)* .2019, 1930-1933.
18 DENG, S., JIANG, Q., WANG, Y., LU, X. & ZHANG, Y. Relationship between quantitative contrast-enhanced ultrasonography parameters and angiogenesis in primary small hepatocellular carcinoma: A retrospective study. *Medicine*, **2021**, 100.
19 DONG, F., AN, J., ZHANG, J., YIN, J., GUO, W., WANG, D., FENG, F., HUANG, S., ZHANG, J. & CHENG, H. Blinking Acoustic Nanodroplets Enable Fast Super-resolution Ultrasound Imaging. *ACS nano*. **2021**, *15*.
20 DE GRACIA LUX, C., VEZERIDIS, A. M., LUX, J., ARMSTRONG, A. M., SIRSI, S. R., HOYT, K. & MATTREY, R. F. Novel method for the formation of monodisperse superheated perfluorocarbon nanodroplets as activatable ultrasound contrast agents. *RSC Adv*. **2017**, *7*, 48561-48568.
21 SONG, J. Ultrasound microbubble contrast agent–carried chemotherapeutic drug microbubbles. *E3S Web of Conferences.* **2019**. 01015.
22 LEE, H., KIM, H., HAN, H., LEE, M., LEE, S., YOO, H., CHANG, J. H. & KIM, H. Microbubbles used for contrast enhanced ultrasound and theragnosis: a review of principles to applications. *Biomedical Engineering Letters*, **2017**, *7,* 59-69.
23 HU, Y. Z., ZHU, J. A., JIANG, Y. G. & HU, B. Ultrasound microbubble contrast agents: application to therapy for peripheral vascular disease. *Adv Ther***. 2009,** *26*, 425-434.
24 SONTUM, P. C. Physicochemical characteristics of Sonazoid™, a new contrast agent for ultrasound imaging. *Ultrasound in medicine & biology*, **2008**, *34*, 824-833.
25 CHUNG, Y. E. & KIM, K. W. Contrast-enhanced ultrasonography: advance and current status in abdominal imaging. *Ultrasonography*, **2015,** *34*, 3.
26 FRINKING, P., SEGERS, T., LUAN, Y. & TRANQUART, F. Three Decades of Ultrasound Contrast Agents: A Review of the Past, Present and Future Improvements. *Ultrasound Med Biol* .**2020**, *46*, 892-908.
27 EMANUEL, A. L., MEIJER, R. I., VAN POELGEEST, E., SPOOR, P., SERNE, E. H. & ERINGA, E. C. Contrast-enhanced ultrasound for quantification of tissue perfusion in humans. *Microcirculation*. **2020** ,*27*, 12588.
28 LIN, H., CHEN, J. & CHEN, C. A novel technology: microfluidic devices for microbubble ultrasound contrast agent generation. *Med Biol Eng Comput.* **2016**, *54*, 1317-1330.

29 COX, K., SEVER, A., JONES, S., WEEKS, J., MILLS, P., DEVALIA, H., FISH, D. & JONES, P. Validation of a technique using microbubbles and contrast enhanced ultrasound (CEUS) to biopsy sentinel lymph nodes (SLN) in pre-operative breast cancer patients with a normal grey-scale axillary ultrasound. *European Journal of Surgical Oncology the Journal of the European Society of Surgical Oncology & the British Association of Surgical Oncology,* **2013**, 39, 760-765
30 SIRSI, S. R. & BORDEN, M. A. Advances in ultrasound mediated gene therapy using microbubble contrast agents. *Theranostics,* **2012**, *2*, 1208-1222.
31 LAHTINEN, O., VANNINEN, R. & RAUTIAINEN, S. Contrast-enhanced ultrasound: a new tool for imaging the superficial lymphatic vessels of the upper limb. *European Radiology Experimental*, **2022,** *6*, 1-9.
32 KARALKO, A., KEŠA, P., JELíNEK, F., ŠEFC, L., JEŽEK, J., ZEMáNEK, P. & GRUS, T. In Vivo Contrast Imaging of Rat Heart with Carbon Dioxide Foam. *Sensors*, **2022**, *22*, 5124.
33 LEA-BANKS, H., MENG, Y., WU, S.-K., BELHADJHAMIDA, R., HAMANI, C. & HYNYNEN, K. Ultrasound-sensitive nanodroplets achieve targeted neuromodulation. *Journal of Controlled Release*, **2021**, *332*, 30-39.
34 SHEERAN, P. S., YOO, K., WILLIAMS, R., YIN, M., FOSTER, F. S. & BURNS, P. N. More than bubbles: creating phase-shift droplets from commercially available ultrasound contrast agents. *Ultrasound in medicine & biology*, **2017**, *43*, 531-540.
35 ZHANG, G., YE, H.-R., SUN, Y. & GUO, Z.-Z. Ultrasound Molecular Imaging and Its Applications in Cancer Diagnosis and Therapy. *ACS Sensors*, **2022**, *7*, 2857-2864.
36 BOURDEAU, R. W., LEE-GOSSELIN, A., LAKSHMANAN, A., FARHADI, A., KUMAR, S. R., NETY, S. P. & SHAPIRO, M. G. Acoustic reporter genes for noninvasive imaging of microorganisms in mammalian hosts. *Nature,* **2018,** *553,* 86-90.
37 HURT, R. C., BUSS, M. T., DUAN, M., WONG, K., YOU, M. Y., SAWYER, D. P., SWIFT, M. B., DUTKA, P., BARTUREN-LARREA, P. & MITTELSTEIN, D. R. Genomically mined acoustic reporter genes for real-time in vivo monitoring of tumors and tumor-homing bacteria. *Nature Biotechnology*, **2023**, 1-13.
38 KEE, A. & TEO, B. M. Biomedical applications of acoustically responsive phase shift nanodroplets: current status and future directions. *Ultrasonics Sonochemistry***, 2019.**
39 ZHANG, G. Nanodroplet-based ultrasound and photoacoustic super-resolution and functional imaging, **2019**
40 AN, J., ZHANG, J., DONG, F., YIN, J., FENG, F., GUO, W., HUANG, S., WANG, D., DANG, J. & ZHANG, J. Arterial Labeling Ultrasound Subtraction Angiography (ALUSA) Based on Acoustic Phase-Change Nanodroplets. *Small*, **2022**, *18,* 2105989.
41 HINGOT, V., ERRICO, C., HEILES, B., RAHAL, L., TANTER, M. & COUTURE, O. Microvascular flow dictates the compromise between spatial resolution and acquisition time in Ultrasound Localization Microscopy. *Scientific Reports*, **2019**, *9*, 2456.
42 RIEMER, K., TOULEMONDE, M., YAN, J., LERENDEGUI, M., STRIDE, E., WEINBERG, P. D., DUNSBY, C. & TANG, M. X. Fast and selective super-resolution ultrasound in vivo with sono-switchable nanodroplets. *IEEE Trans Med Imaging*. **2022**.
43 COUTURE, O., HINGOT, V., HEILES, B., MULEKI-SEYA, P. & TANTER, M. Ultrasound localization microscopy and super-resolution: A state of the art. *IEEE transactions on ultrasonics, ferroelectrics, and frequency control,* **2018,** *65*, 1304-1320.
44 GUO, R., XU, N., LIU, Y., LING, G., YU, J. & ZHANG, P. Functional ultrasound-triggered

phase-shift perfluorocarbon nanodroplets for cancer therapy. *Ultrasound in Medicine & Biology,* **2021**, *47*, 2064-2079.
45 ZHANG, G., HARPUT, S., HU, H., CHRISTENSEN-JEFFRIES, K., ZHU, J., BROWN, J., LEOW, C. H., ECKERSLEY, R. J., DUNSBY, C. & TANG, M.-X. Fast Acoustic Wave Sparsely Activated Localization Microscopy: Ultrasound Super-Resolution Using Plane-Wave Activation of Nanodroplets. *IEEE Transactions on Ultrasonics, Ferroelectrics, and Frequency Control*, **2019**, *66*, 1039-1046.
46 MANNARIS, C., YANG, C., CARUGO, D., OWEN, J., LEE, J. Y., NWOKEOHA, S., SETH, A. & TEO, B. M. Acoustically responsive polydopamine nanodroplets: a novel theranostic agent. *Ultrasonics sonochemistry*, **2020**, *60*, 104782.
47 ZHU, Y. I., YOON, H., ZHAO, A. X. & EMELIANOV, S. Y. Leveraging the Imaging Transmit Pulse to Manipulate Phase-Change Nanodroplets for Contrast-Enhanced Ultrasound. *IEEE Transactions on Ultrasonics, Ferroelectrics, and Frequency Control*, **2019**, *66*, 692-700.
48 HANNAH, A. S., LUKE, G. P. & EMELIANOV, S. Y. Blinking Phase-Change Nanocapsules Enable Background-Free Ultrasound Imaging. *Theranostics*, **2016**, *6,* 1866-1876.
49 BAE, Y. H. & PARK, K. Targeted drug delivery to tumors: myths, reality and possibility. *Journal of controlled release,* **2011**, *153*, 198.
50 LIN, C.-Y. & PITT, W. G. Acoustic droplet vaporization in biology and medicine. *BioMed research international.* **2013.**
51 RAPOPORT, N., GUPTA, R., KIM, Y.-S. & O'NEILL, B. E. Polymeric micelles and nanoemulsions as tumor-targeted drug carriers: insight through intravital imaging. *Journal of Controlled Release,* **2015**, *206*, 153-160.
52 SONG, R., ZHANG, C., TENG, F., TU, J., GUO, X., FAN, Z., ZHENG, Y. & ZHANG, D. Cavitation-facilitated transmembrane permeability enhancement induced by acoustically vaporized nanodroplets. *Ultrason Sonochem*. **2021** ,*79*, 105790.
53 CAO, Y., CHEN, Y., YU, T., GUO, Y., LIU, F., YAO, Y., LI, P., WANG, D., WANG, Z. & CHEN, Y. Drug release from phase-changeable nanodroplets triggered by low-intensity focused ultrasound. *Theranostics*, **2018**, *8*, 1327.
54 HO, Y.-J. & YEH, C.-K. Concurrent anti-vascular therapy and chemotherapy in solid tumors using drug-loaded acoustic nanodroplet vaporization. *Acta Biomaterialia*. **2017** ,*49*, 472-485.
55 LEA-BANKS, H. & HYNYNEN, K. Sub-millimetre precision of drug delivery in the brain from ultrasound-triggered nanodroplets. *Journal of Controlled Release*, **2021**, *338*, 731-741.
56 XU, T., CUI, Z., LI, D., CAO, F., XU, J., ZONG, Y., WANG, S., BOUAKAZ, A., WAN, M. & ZHANG, S. Cavitation characteristics of flowing low and high boiling-point perfluorocarbon phase-shift nanodroplets during focused ultrasound exposures. *Ultrasonics sonochemistry*. **2020**, *65*, 105060.
57 MCHUGH, C. T., DURHAM, P. G., ATALLA, S., KELLEY, M., BRYDEN, N. J., DAYTON, P. A. & BRANCA, R. T. Low-boiling Point Perfluorocarbon Nanodroplets as Dual-Phase Dual-Modality MR/US Contrast Agent. *ChemPhysChem*. **2022**, *23*, e202200438.
58 DERUITER, R. M., MARKLEY, E. N., ROJAS, J. D., PINTON, G. F. & DAYTON, P. A. Transient acoustic vaporization signatures unique to low boiling point phase change contrast agents enable super-resolution ultrasound imaging without spatiotemporal filtering. *AIP Adv***.2020**, *10,* 105124.
59 LIU, W. W., WU, C. T., WANG, C. & LI, P. C. Acoustic and optical droplet vaporization for

enhanced sonoporation. 2016 *IEEE International Ultrasonics Symposium (IUS)*, **2016**.
60 KIM, J., DERUITER, R. M., GOEL, L., XU, Z., JIANG, X. & DAYTON, P. A. A Comparison of Sonothrombolysis in Aged Clots between Low-Boiling-Point Phase-Change Nanodroplets and Microbubbles of the Same Composition. *Ultrasound in medicine & biology* ,**2020**, *46*, 3059-3068.
61 LUKE, G. P., HANNAH, A. S. & EMELIANOV, S. Y. Super-resolution ultrasound imaging in vivo with transient laser-activated nanodroplets. *Nano letters*. **2016**, *16*, 2556-2559.
62 SHEERAN, P. S., WONG, V. P., LUOIS, S., MCFARLAND, R. J., ROSS, W. D., FEINGOLD, S., MATSUNAGA, T. O. & DAYTON, P. A. Decafluorobutane as a phase-change contrast agent for low-energy extravascular ultrasonic imaging. *Ultrasound in medicine & biology,* **2011**, *37,* 1518-1530.
63 ZHANG, G., LIN, S., LEOW, C. H., PANG, K., HERNáNDEZ-GIL, J., CHEE, M., LONG, N. J., MATSUNAGA, T. O. & TANG, M.-X. Acoustic response of targeted nanodroplets post-activation using high frame rate imaging. *IEEE International Ultrasonics Symposium (IUS)*, **2017**, 1-4.
64 DURHAM, P. G. & DAYTON, P. A. Applications of sub-micron low-boiling point phase change contrast agents for ultrasound imaging and therapy. *Current Opinion in Colloid & Interface Science* ,**2021**, 56, 101498.
65 YOON, H. Ultrasound and Photoacoustic Imaging of Laser-Activated Phase-Change Perfluorocarbon Nanodroplets. *Photonics*. **2021**, 405.
66 ZHANG, G., HARPUT, S., HU, H., CHRISTENSEN-JEFFRIES, K., ZHU, J., BROWN, J., LEOW, C. H., DUNSBY, C., ECKERSLEY, R. J. & TANG, M.-X. Fast Acoustic Wave Sparsely Activated Localization Microscopy (Fast-AWSALM) Using Octafluoropropane N Anodroplets. *IEEE International Ultrasonics Symposium (IUS)***, 2018**, 1-9.
67 YOON, H., HALLAM, K. A., YOON, C. & EMELIANOV, S. Y. Super-resolution imaging with ultrafast ultrasound imaging of optically triggered perfluorohexane nanodroplets. *IEEE transactions on ultrasonics, ferroelectrics, and frequency control* ,**2018**, *65*, 2277-2285.
68 ZHANG, G., HARPUT, S., ZHU, J., CHRISTENSEN-JEFFRIES, K., BROWN, J., LEOW, C. H., DUNSBY, C., ECKERSLEY, R. J. & TANG, M.-X. Minimization of nanodroplet activation time using focused-pulses for droplet-based ultrasound super-resolution imaging. *IEEE International Ultrasonics Symposium (IUS),* **2019**. *pp.* 372-375.
69 YUAN, Z., DEMITH, A., STOFFEL, R., ZHANG, Z. & PARK, Y. C. Light-activated doxorubicin-encapsulated perfluorocarbon nanodroplets for on-demand drug delivery in an in vitro angiogenesis model: Comparison between perfluoropentane and perfluorohexane. *Colloids and Surfaces B: Biointerfaces.* **2019**, *184*.
70 SABUNCU, S., JAVIER RAMIREZ, R., FISCHER, J. M., CIVITCI, F. & YILDIRIM, A. Ultrafast Background-Free Ultrasound Imaging Using Blinking Nanoparticles. *Nano.Lett*. **2023**, *23*, 659-666.
71 CHEN, X., LOWERISON, M. R., DONG, Z., HAN, A. & SONG, P. Deep Learning-Based Microbubble Localization for Ultrasound Localization Microscopy. *IEEE Trans Ultrason Ferroelectr Freq Control* .**2022**, *69*, 1312-1325.
72 ESPINDOLA, D., DERUITER, R. M., SANTIBANEZ, F., DAYTON, P. A. & PINTON, G. Quantitative sub-resolution blood velocity estimation using ultrasound localization microscopy ex-vivo and in-vivo. *Biomed. Phys .Eng .Express* .**2020,** *6*, 035019.
73 DESAILLY, Y., PIERRE, J., COUTURE, O. & TANTER, M. Resolution limits of ultrafast

ultrasound localization microscopy. *Phys. Med. Biol*. **2015**, *60,* 8723-8740.
74 LOK, U. W., HUANG, C., TRZASKO, J. D., KIM, Y., LUCIEN, F., TANG, S., GONG, P., SONG, P. & CHEN, S. Three-Dimensional Ultrasound Localization Microscopy with Bipartite Graph-Based Microbubble Pairing and Kalman-Filtering-Based Tracking on a 256-Channel Verasonics Ultrasound System with a 32 × 32 Matrix Array. *Journal of Medical and Biological Engineering*, **2022**, *42,* 767-779.
75 LIU, X., ZHOU, T., LU, M., YANG, Y., HE, Q. & LUO, J. Deep Learning for Ultrasound Localization Microscopy. *IEEE. Trans. Med. Imaging*. **2020,** *39*, 3064-3078.
76 HEILES, B., CORREIA, M., HINGOT, V., PERNOT, M., PROVOST, J., TANTER, M. & COUTURE, O. Ultrafast 3D Ultrasound Localization Microscopy Using a 32 x 32 Matrix Array. *IEEE. Trans. Med. Imaging*. **2019**, *38*, 2005-2015.
77 ZHANG, G., TOULEMONDE, M., RIEMER, K., ZHU, J., HARPUT, S., CHRISTENSEN-JEFFRIES, K., ZHU, Z., WANG, B., LEOW, C. H. & WEINBERG, P. Effects of Mechanical Index on Repeated Sparse Activation of Nanodroplets In Vivo. *IEEE International Ultrasonics Symposium (IUS)*, **2020**, 1-4.
78 LIN, F., SHELTON, S. E., ESPíNDOLA, D., ROJAS, J. D., PINTON, G. & DAYTON, P. A. 3-D Ultrasound Localization Microscopy for Identifying Microvascular Morphology Features of Tumor Angiogenesis at a Resolution Beyond the Diffraction Limit of Conventional Ultrasound. Theranostics. **2017**, 7, 196-204.
79 FIALA, C. & DIAMANDIS, E. P. Utility of circulating tumor DNA in cancer diagnostics with emphasis on early detection. BMC. Med, **2018**, 16, 166.
80 LEI, Y. M., YIN, M., YU, M. H., YU, J. & DIETRICH, C. F. Artificial Intelligence in Medical Imaging of the Breast. Frontiers in Oncology, **2021**, 11, 600557.
81 LOWERISON, M., ZHANG, W., CHEN, X., FAN, T. & SONG, P. Characterization of Anti-Angiogenic Chemo-Sensitization via Longitudinal Ultrasound Localization Microscopy in Colorectal Carcinoma Tumor Xenografts. IEEE Trans. Biomed. Eng. **2022,** 69, 1449-1460.
82 BAR-ZION, A., SOLOMON, O., TREMBLAY-DARVEAU, C., ADAM, D. & ELDAR, Y. C. SUSHI: Sparsity-based ultrasound super-resolution hemodynamic imaging. IEEE transactions on ultrasonics, ferroelectrics, and frequency control. **2018**, 65, 2365-2380.
83 F. LIN, E. A. Super resolution contrast ultrasound imaging: Analysis of imaging resolution and application to imaging tumor angiogenesis. IEEE International Ultrasonics Symposium (IUS), **2016.**
84 HUI-MING, Y. I., RLOWERISON, M., SONG, P. F. & ZHANG, W. A Review of Clinical Applications for Super-resolution Ultrasound Localization Microscopy. Current Medical Science, **2022**, 42, 16.
85 ZHU, J., ROWLAND, E. M., HARPUT, S., RIEMER, K., LEOW, C. H., CLARK, B., and others 3D Super-Resolution US Imaging of Rabbit Lymph Node Vasculature in Vivo by Using Microbubbles. Radiology, **2019**, 291, 642-650.
86 LOWERISON, M. R., HUANG, C., LUCIEN, F., CHEN, S. & SONG, P. Ultrasound localization microscopy of renal tumor xenografts in chicken embryo is correlated to hypoxia. Sci. Rep. **2020**, 10, 2478.
87 GE ZHANG, J. Y., YU-MENG LEI , JUN-RUI HU ,HAI-MAN HU , SEVAN HARPUT,ZHEN-ZHONG GUO ,XIN-WU CUI,HUA-RONG YE Ultrasound super-resolution imaging for the differential diagnosis of thyroid nodules: A pilot study. Front. Oncol. **2022**, 12, 978164.

88 ZHANG, G., LEI, Y.-M., LI, N., YU, J., JIANG, X.-Y., YU, M.-H., HU, H.-M., ZENG, S.-E., CUI, X.-W. & YE, H.-R. Ultrasound super-resolution imaging for differential diagnosis of breast masses. Frontiers in Oncology, **2022**, 12.
89 OPACIC, T., DENCKS, S., THEEK, B., PIEPENBROCK, M., ACKERMANN, D., RIX, A., LAMMERS, T., STICKELER, E., DELORME, S., SCHMITZ, G. & KIESSLING, F. Motion model ultrasound localization microscopy for preclinical and clinical multiparametric tumor characterization. Nat.Commun**. 2018**, 9, 1527.
90 GHOSH, D., XIONG, F., SIRSI, S. R., MATTREY, R., BREKKEN, R., KIM, J.-W. & HOYT, K. Monitoring early tumor response to vascular targeted therapy using super-resolution ultrasound imaging. IEEE international ultrasonics symposium (Ius), **2017,** 1-4.
91 ZHANG, G., WANG, B., SHAH, A., BAMBER, J. & TANG, M. X. Contrast-Enhanced Photoacoustic Imaging of Low-boiling-point Phase-Change Nanodroplets. 2019 IEEE International Ultrasonics Symposium (IUS), **2019**.
92 ZHANG, J., LI, N., DONG, F., LIANG, S., WANG, D., AN, J., LONG, Y., WANG, Y., LUO, Y. & ZHANG, J. Ultrasound Microvascular Imaging Based on Super-Resolution Radial Fluctuations. Journal of Ultrasound in Medicine, **2020**, 39, 1507-1516.
93 LIN, F., TSURUTA, J. K., ROJAS, J. D. & DAYTON, P. A. Optimizing Sensitivity of Ultrasound Contrast-Enhanced Super-Resolution Imaging by Tailoring Size Distribution of Microbubble Contrast Agent. Ultrasound. Med. Biol. **2017**, 43, 2488-2493.
94 CHEN, Q., YU, J., LUKASHOVA, L., LATOCHE, J. D., ZHU, J., LAVERY, L., VERDELIS, K., ANDERSON, C. J. & KIM, K. Validation of Ultrasound Super-Resolution Imaging of Vasa Vasorum in Rabbit Atherosclerotic Plaques. IEEE Trans Ultrason Ferroelectr Freq Control. **2020**, 67, 1725-1729.
95 QIAN, X., HUANG, C., LI, R., SONG, B. J., TCHELEPI, H., SHUNG, K. K., CHEN, S., HUMAYUN, M. S. & ZHOU, Q. Super-resolution ultrasound localization microscopy for visualization of the ocular blood flow. IEEE Transactions on Biomedical Engineering, **2021**, 69, 1585-1594.
96 GHOSH, D., PENG, J., BROWN, K., SIRSI, S., MINEO, C., SHAUL, P. W. & HOYT, K. Super-Resolution Ultrasound Imaging of Skeletal Muscle Microvascular Dysfunction in an Animal Model of Type 2 Diabetes. J. Ultrasound. Med. **2019**, 38, 2589-2599.
97 CHEN, Q., YU, J., RUSH, B. M., STOCKER, S. D., TAN, R. J. & KIM, K. Ultrasound super-resolution imaging provides a noninvasive assessment of renal microvasculature changes during mouse acute kidney injury. Kidney Int. **2020**, 98, 355-365.
98 LOWERISON, M. R., SEKARAN, N. V. C., ZHANG, W., DONG, Z., CHEN, X., LLANO, D. A. & SONG, P. Aging-related cerebral microvascular changes visualized using ultrasound localization microscopy in the living mouse. Sci. Rep. **2022**, 12, 619.
99 HARPUT, S., CHRISTENSEN-JEFFRIES, K., BROWN, J., LI, Y., WILLIAMS, K. J., DAVIES, A. H., and others Two-Stage Motion Correction for Super-Resolution Ultrasound Imaging in Human Lower Limb. IEEE .Trans .Ultrason .Ferroelectr. Freq.Control. **2018** ,65, 803-814.
100 HUANG, C., ZHANG, W., GONG, P., LOK, U. W., TANG, S., YIN, T., ZHANG, X., ZHU, L., SANG, M., SONG, P., ZHENG, R. & CHEN, S. Super-resolution ultrasound localization microscopy based on a high frame-rate clinical ultrasound scanner: an in-human feasibility study. Phys. Med. Biol. **2021**, 66.

101 DEMENé, C., ROBIN, J., DIZEUX, A., HEILES, B., PERNOT, M., TANTER, M. & PERREN, F. Transcranial ultrafast ultrasound localization microscopy of brain vasculature in patients. Nature biomedical engineering, **2021**, 5, 219-228.
102 GOUDOT, G., JIMENEZ, A., MOHAMEDI, N., SITRUK, J., KHIDER, L., MORTELETTE, H., PAPADACCI, C., HYAFIL, F., TANTER, M. & MESSAS, E. Assessment of Takayasu's arteritis activity by ultrasound localization microscopy. Ebiomedicine, **2023**, 90.
103 BORDY, R., TOTOSON, P., PRATI, C., MARIE, C., WENDLING, D. & DEMOUGEOT, C. Microvascular endothelial dysfunction in rheumatoid arthritis. Nat. Rev. Rheumatol. **2018**, 14, 404-420.
104 LEE, H., LEE, M. Y., BHANG, S. H., KIM, B. S., KIM, Y. S., JU, J. H., KIM, K. S. & HAHN, S. K. Hyaluronate-gold nanoparticle/tocilizumab complex for the treatment of rheumatoid arthritis. ACS. Nano. **2014,** 8, 4790-4798.
105 LEE, H., LEE, K., KIM, I. K. & PARK, T. G. Synthesis, characterization, and in vivo diagnostic applications of hyaluronic acid immobilized gold nanoprobes. Biomaterials, **2008**, 29, 4709-4718.
106 JEONG, E. H., JUNG, G., HONG, C. A. & LEE, H. Gold nanoparticle (AuNP)-based drug delivery and molecular imaging for biomedical applications. Archives of pharmacal research, **2014,** 37, 53-59.
107 OLIVEIRA, I. M., GONçALVES, C., REIS, R. L. & OLIVEIRA, J. M. Engineering nanoparticles for targeting rheumatoid arthritis: Past, present, and future trends. Nano Research. **2018**, 11, 4489-4506.
108 LI, R., HE, Y., ZHU, Y., JIANG, L., ZHANG, S., QIN, J., WU, Q., DAI, W., SHEN, S., PANG, Z. & WANG, J. Route to Rheumatoid Arthritis by Macrophage-Derived Microvesicle-Coated Nanoparticles. Nano, Lett. **2019**, 19, 124-134.
109 DOLATI, S., SADREDDINI, S., ROSTAMZADEH, D., AHMADI, M., JADIDI-NIARAGH, F. & YOUSEFI, M. Utilization of nanoparticle technology in rheumatoid arthritis treatment. Biomed Pharmacother. **2016**, 80, 30-41.
110 LEE, S. M., KIM, H. J., HA, Y. J., PARK, Y. N., LEE, S. K., PARK, Y. B. & YOO, K. H. Targeted chemo-photothermal treatments of rheumatoid arthritis using gold half-shell multifunctional nanoparticles. ACS Nano. **2013**, 7, 50-57.
111 DEMEULENAERE, O., BERTOLO, A., PEZET, S., IALY-RADIO, N., OSMANSKI, B., PAPADACCI, C., TANTER, M., DEFFIEUX, T. & PERNOT, M. In vivo whole brain microvascular imaging in mice using transcranial 3D Ultrasound Localization Microscopy. EBioMedicine, **2022**, 79, 103995.
112 YIN, J., ZHANG, J., ZHU, Y., DONG, F., AN, J., WANG, D., LI, N., LUO, Y., WANG, Y. & WANG, X. Ultrasound microvasculature imaging with entropy-based radiality super-resolution (ERSR). Physics in Medicine & Biology, **2021**, 66, 215012.
113 CHEN, Q., SONG, H., YU, J. & KIM, K. Current development and applications of super-resolution ultrasound imaging. Sensors, **2021**, 21, 2417.
114 SONG, P., TRZASKO, J. D., MANDUCA, A., HUANG, R., KADIRVEL, R., KALLMES, D. F. & CHEN, S. Improved super-resolution ultrasound microvessel imaging with spatiotemporal nonlocal means filtering and bipartite graph-based microbubble tracking. IEEE transactions on ultrasonics, ferroelectrics, and frequency control, **2017**, 65, 149-167.

115 CHRISTENSEN-JEFFRIES, K., BROWNING, R. J., TANG, M. X., DUNSBY, C. & ECKERSLEY, R. J. In vivo acoustic super-resolution and super-resolved velocity mapping using microbubbles. IEEE Trans. Med. Imaging. **2015** ,34, 433-440.
116 CHAVIGNON, A., HEILES, B., HINGOT, V., ORSET, C., VIVIEN, D. & COUTURE, O. 3D Transcranial Ultrasound Localization Microscopy in the Rat Brain With a Multiplexed Matrix Probe. IEEE Trans. Biomed. Eng. **2022**, 69, 2132-2142.
117 VAN SLOUN, R. J., SOLOMON, O., BRUCE, M., KHAING, Z. Z., WIJKSTRA, H., ELDAR, Y. C. & MISCHI, M. Super-resolution ultrasound localization microscopy through deep learning. IEEE transactions on medical imaging, **2020**, 40, 829-839.
118 HARPUT, S., FONG, L. H., STANZIOLA, A., ZHANG, G., TOULEMONDE, M., ZHU, J., CHRISTENSEN-JEFFRIES, K., BROWN, J., ECKERSLEY, R. J. & GRISAN, E. Super-resolution ultrasound image filtering with machine-learning to reduce the localization error. IEEE International Ultrasonics Symposium (IUS), **2019**, 2118-2121.
119 NYANKIMA, A. G., ROJAS, J. D., CIANCIOLO, R., JOHNSON, K. A. & DAYTON, P. A. In vivo assessment of the potential for renal bio-effects from the vaporization of perfluorocarbon phase-change contrast agents. *Ultrasound in medicine & biology,* **2018**, *44*, 368-376.
for TOC only: